Competitive ion-exchange reactions of Pb(II) (Pb2+/PbCl+) and Ra(II) (Ra2+) on smectites: Experiments, modeling, and implication for 226Ra(II)/210Pb(II) disequilibrium in the environment.

Flora Parrotin, Valentin Robin, Catherine Beaucaire, Michael Descostes, Emmanuel Tertre

Competitive ion-exchange reactions of Pb(II) (Pb^{2+}/$PbCl^{+}$) and Ra(II) (Ra^{2+}) on smectites: experiments, modeling, and implication for $^{226}Ra(II)/^{210}Pb(II)$ disequilibrium in the environment.

Flora PARROTIN[1,2,3*], Valentin ROBIN[2], Catherine BEAUCAIRE[4,#], Michael DESCOSTES[3,5], Emmanuel TERTRE[1]

[1] IC2MP, Equipe HydrASA, UMR 7285 CNRS/Université de Poitiers, 86073 Poitiers, France.
[2] E2Lim, UR 24 133, Université de Limoges, 123 avenue Albert Thomas, 87060 Limoges Cedex, France
[3] Orano Mining, Environmental R&D Dpt., 125 avenue de Paris, 92320 Chatillon, France
[4] CEA, Centre d'Etudes de Saclay, DANS/DPC/SECR/L3MR, 91191 Gif sur Yvette, France
[5] Centre de Géosciences, MINES ParisTech, PSL University, 35 rue St Honoré, 77300 Fontainebleau, France
[#]Present address: [e] Consultant, 21540 Chevannay, France

[*] E-mail address of the corresponding author:
Flora PARROTIN: flora.parrotin@univ-poitiers.fr

Graphical abstract

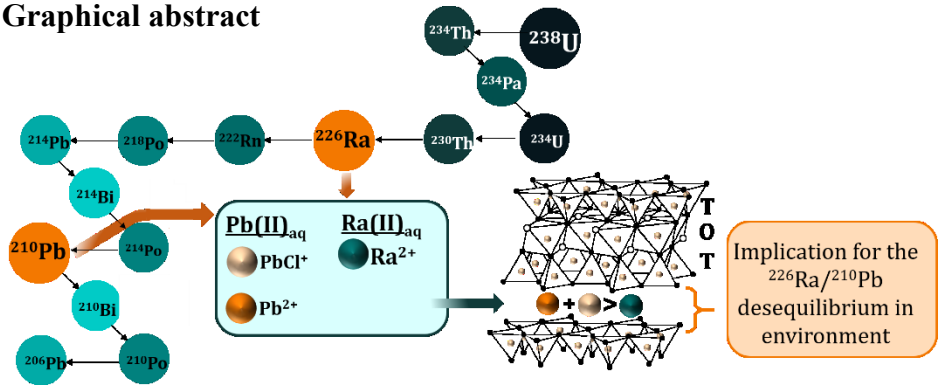

Highlights

- Reliable multisite ion-exchange model for Pb^{2+} and $PbCl^{+}$ on swelling clay minerals
- Preferential adsorption on clay minerals of $PbCl^{+}$ ion pairs compared to Pb^{2+}
- $^{226}Ra/^{210}Pb$ disequilibrium evidenced due to selective adsorption on smectite

Keywords

Ion-exchange, ion pairs, lead, radium, radioactive disequilibrium, smectite

Abstract

In this study, new experimental data for the adsorption of lead onto a swelling clay mineral with a tetrahedral charge (beidellite) at the ultratrace level ($<10^{-10}$ mol/L) are presented. The data were interpreted using an ion-exchange multisite model that considers the sorption of major cations (including H^+), which always compete with trace elements for sorption onto mineral surfaces in natural environments. The ability of the proposed model to predict experimental K_d values under various conditions of ionic strength (fixed by NaCl solutions) and aqueous cation compositions (including Pb^{2+} and $PbCl^+$) was tested. The proposed model was applied to experimental data previously published for other types of swelling clay minerals, and the results were compared with the results obtained using previously published models. The preferential adsorption of chloride ion pairs, as well as the effect of the swelling clay crystal chemistry on lead adsorption, were assessed. Finally, the selective adsorption behavior of ^{226}Ra compared to ^{210}Pb was demonstrated, which has implications for the study of many environmental processes using isotope partitioning.

1. Introduction

^{238,235}U-series and ^{232}Th disequilibria have been used for several decades in the field of geosciences (see reviews made by (Broecker and Peng, 1982; Ivanovich and Harmon, 1992) and references therein). Early decay chain isotopes (^{238,235,234}U, ^{231}Pa, ^{234,232,230,228}Th, ^{226}Ra) are generally used for dating and highlighting geochemical processes (Grozeva et al., 2022; Milena-Pérez et al., 2021; Vigier et al., 2001). For example, the use of end members of the U decay chain, such as ^{226}Ra (half-life 1600 y) and ^{210}Pb (half-life 22.2 y), constrains shorter durations of geological events, such as volcanic eruptions or coral growth (Berlo and Turner, 2010; Ghaleb, 2009; Love et al., 2007; Mabit et al., 2014; Moore and Krishnaswami, 1972; Pickler et al., 2012; Rihs et al., 2021; Wang et al., 2019). In this approach, the assumption is made that geological systems are closed, leading to secular equilibrium between ^{226}Ra and ^{210}Pb (i.e., their activities are equal).

Hence, in applications such as dating of recent deposits using radionuclides as well as radioactive waste disposal management, water resource assessment and remediation of mining environments, it is important to understand and predict the mobility of lead at trace levels (Kelebemang et al., 2017; Lacal et al., 2003; MacKenzie et al., 1998). In natural environments, predicting the concentration of aqueous lead (i.e., Pb(II)) in natural waters and its mobility is challenging due to the many chemical processes in which this element is involved, such as: (i) precipitation or coprecipitation in carbonates and in sulfate-bearing minerals when oxidizing conditions prevail (Fu et al., 2020), (ii) precipitation in sulfide minerals in reducing conditions (Fagbohungbe et al., 2017; Lacal et al., 2003), and (iii) adsorption/ion-exchange on clay minerals (Tabelin et al., 2020; Uddin, 2017) and oxyhydroxides of Fe- Mn (Serpaud et al., 1994). At high aqueous concentrations (>10^{-5} M) under oxidized conditions (site-specific), aqueous Pb(II) is controlled by carbonate and/or sulfate precipitation (Marani et al., 1995; Orucoglu, et al., 2018). For lower concentrations, with undersaturation of the solution with regard to pure lead phases, control is assured by coprecipitation in sulfates (Curti et al., 2010; Hanor, 2000; Ram et al., 2021; Zhu et al., 2004) and adsorption/ion-exchange on soil or sediment components (e.g., clays and Fe-Mn oxyhydroxides) (Hem, 1976).

Using radioactive tracers such as ^{210}Pb at trace levels is also a way to study the ion-exchange reactions (i.e., reversible adsorption) of Pb(II) (by assuming no isotope fractionation), as the total concentration used is far below the solubility of potential newly formed minerals. The occurrence of ^{210}Pb in surface and subsurface environments may also be due to the presence of uranium ore deposits or radioactive waste disposal. Except in the specific case of U-rich ores, and even though secular equilibrium in the rock is reached (i.e., massic activities of all isotopes

in a radioactive decay chain are equal), concentrations of ^{210}Pb, from the decay of ^{238}U, are at trace levels in most of the natural rocks (typically <0.1 wt%). These low values lead to extremely low aqueous concentrations of ^{210}Pb in most of the natural waters in contact with these rocks (<40 mBq/L, i.e., $<10^{-18}$ M) (Persson and Holm, 2011).

While many studies have been published on the geochemical reactivity of ^{226}Ra (Billon et al., 2020; Bordelet et al., 2018; Langmuir and Riese, 1985; Lestini et al., 2019; Reiller and Descostes, 2020; Reinoso-Maset and Ly, 2016; Robin et al., 2017; Sajih et al., 2014), the fate of ^{210}Pb is usually linked to the chemical properties of Pb element, at very low concentrations. In most studies related to date geological processes, no chemical reactivity (or at least the same chemical reactivity) is assumed for both elements (Pb(II) and Ra(II)) (Berlo and Turner, 2010; Ghaleb, 2009; Love et al., 2007; Mabit et al., 2014; Moore and Krishnaswami, 1972; Pickler et al., 2012). This last assumption has to be assessed especially because: (i) in oxidizing conditions, Pb(II) can easily form insoluble carbonate and sulfate minerals at high Pb aqueous concentrations (10^{-5} M), while it is not the case for Ra(II), which is only radiogenic and then presents only at very low concentrations in rocks or soils (usually <0.88 ppt) and in natural waters ($<10^{-15}$ M) (Fesenko et al., 2014), and (ii) aqueous speciation of both elements is generally significantly different in natural waters (Fesenko et al., 2014; Powell et al., 2009). Indeed, for example, Ra(II) is generally only present as Ra^{2+} and $RaSO_4$, while Pb(II) can preferentially form aqueous complexes with anionic species such as Cl^- (as $PbCl^+$ and $PbCl_{2(aq)}$) but also carbonate and sulfate, which are major inorganic anions in natural waters (Reiller and Descostes, 2020; Robin et al., 2017).

Clay minerals are very common in all surface environments (such as sedimentary basins and soils) (Meunier, 2005) and are well known, especially in swelling minerals (such as smectite), to have high ion-exchange and adsorption properties (McBride, 1994; Pabalan and Turner, 1996). Regarding Pb(II), several studies exist in the literature for smectites (Barbier et al., 2000; Fernandes and Baeyens, 2019; Mbadcam et al., 2011; Mhamdi et al., 2013; Orucoglu et al., 2018; Yin et al., 2018). Nevertheless, very few of them focused: (i) on very low concentrations ($<10^{-6}$ M), which are representative of radiogenic Pb (such as ^{210}Pb), and (ii) on aqueous speciation with Cl^-, which is a significant anion in most natural waters (Powell et al., 2009) and may form metallic chloride complexes ($MeCl^+$) known to be easily adsorbed onto swelling clay minerals (Charlet and Tournassat, 2005; Tertre et al., 2011a, 2011b; Tournassat et al., 2004; Wang et al., 2015, among others). Moreover, no study is available relative to the adsorption properties of both Ra(II) and Pb(II) for the same clay mineral and obtained for identical physicochemical conditions in a chloride medium (pH, ionic strength, presence of

116 competitors), making it difficult to quantitatively predict the possible difference in adsorption
117 properties between the two elements on a given (and same) clay mineral.
118 Then, to assess: (i) the possible difference in the adsorption properties of Ra(II) and Pb(II)
119 for a swelling clay mineral at low aqueous Pb concentrations (i.e., $<10^{-10}$ M), and (ii) discuss
120 these results in the context of ^{226}Ra(II)/^{210}Pb(II) natural disequilibrium measurements, this
121 study will compare adsorption data previously published for Ra(II) (Robin et al., 2017) with
122 those obtained in the present study for Pb(II) for a Na-beideillite (i.e., a low charge swelling
123 clay). This clay mineral is commonly found in natural environments (Robin et al.,2020, 2015a;
124 Zhao et al., 2021), and its ion-exchange properties, based on multiple sites, for the main cations
125 of natural waters (i.e., Na^+, K^+, Ca^{2+} and Mg^{2+}) are also well known (Robin et al., 2015b). This
126 last characteristic allows us to test its predictive capacity in several environmental conditions
127 (Ballini et al., 2020; Besançon et al., 2020; de Boissezon et al., 2020; Robin et al., 2020, 2017).
128 Note that both series of data were obtained using batch experiments in which both elements
129 were present at the same time, allowing us to prevent any physicochemical variations (pH, ionic
130 strength, temperature, etc.) that could make the comparisons difficult between the two series of
131 data. Pb(II) adsorption data, obtained as a function of pH for two NaCl concentrations, will be
132 reported and interpreted considering the previous ion-exchange model obtained for Ra(II) and
133 major cations on the material used (Robin et al., 2017, 2015b), characterized by the same three
134 sorption sites for major and trace element (i.e. without adding a specific site for trace element
135 commonly named “site of low concentration but high affinity in some literature (de Boissezon
136 et al., 2020; Fernandes and Baeyens, 2019)”. Moreover, experimental data were interpreted by
137 taking into account aqueous speciation including chloride-lead complexes (especially $PbCl^+$,
138 which can be adsorbed onto clay minerals (Wang et al., 2015). Data obtained for Pb(II) will
139 then be compared and discussed with previous data found in the literature, and the possible
140 different adsorption properties of the swelling clay for Ra(II) and Pb(II) will be discussed in the
141 context to date geological mechanisms (via ^{226}Ra(II)/^{210}Pb(II) natural disequilibrium
142 measurements).
143
144 **2. Materials and methods**
145 ***2.1. Smectite characterization***
146 Experiments were performed with a dioctahedral smectite, referenced as a beidellite from
147 Silver City, Idaho, USA (SBId-1), having the following structural formula:
148 $(Si_{7.15}Al_{0.85})(Al_{3.62}Mg_{0.18}Fe^{3+}_{0.22})O_{20}(OH)_4M^+_{0.95}$ per unit cell (Gailhanou et al., 2012) and
149 issued from the Society Source Clay Repository (Department of Agronomy, Purdue University,

West Lafayette, IN, USA). Size fractionation was performed on SBId-1 by centrifugation to obtain a <0.3 µm size fraction to limit the possible presence of mineralogical impurities (minor kaolinite and illite/smectite interstratified minerals, <5 wt%) before being dried at 60 °C. Sorption sites were saturated with Na^+ using 3 M NaCl solution, followed by chloride removal by dialysis before drying at 60 °C. The specific surface area (SSA) of external surfaces and the total cation exchange capacity (CEC) are approximately 70 m^2/g and 100 meq/100 g, respectively (more information can be found in (Robin et al., 2017, 2015b).

2.2. Ion-exchange experiments

^{210}Pb adsorption and desorption experiments were performed at the same time as the ^{226}Ra experiments presented in Robin et al. (2017), which allows discussion of radioactive disequilibrium. Experiments were performed as a function of pH with values adjusted by the addition of HCl or NaOH to obtain a pH range from 2.2 to 7.3 at equilibrium. Experiments were performed at two ionic strengths ($[Cl]_{tot.}$=0.11 M and 0.027 M fixed by NaCl solutions; $[Cl]_{tot.}$ is the term used later in this study to discuss the ionic strengths effects). HCl and NaOH additions were considered in the calculation of total Na^+ and Cl^- contents) with a solid/liquid ratio of 2.78 g/L in 10 mL Nalgene™ centrifuge tubes. This solid solution ratio is commonly used in literature (Fernandes and Baeyens, 2019; Orucoglu et al., 2018; Tertre et al., 2011a; Robin et al., 2015b); using higher ratio would induce possible problem accessibility of solute to the solid surface and a lower solid solution ratio could lead to higher analytical uncertainties to quantify sorption. After equilibration for 2 days between the solid (SBId-1) and the NaCl solutions, either 50 or 90 µL (±5 µL) of 13.0 kBq/mL ^{210}Pb and 72.9 kBq/mL ^{226}Ra ($^{226}Ra(NO_3)_2$ solution, Isotope Products Laboratories, USA; the source concentration was controlled by γ-ray spectrometry) was added to each batch experiment. The initial measured activity of ^{210}Pb in the solution ranged from 60 to 135 Bq/mL, i.e., $1{\cdot}10^{-10}$ to $2.3{\cdot}10^{-10}$ M and the one of ^{226}Ra from 300 to 700 Bq/mL, i.e., $4{\cdot}10^{-8}$ to $8.5{\cdot}10^{-8}$ M. After adding the lead solution, the centrifuge tubes were continuously shaken using a mixing rotor for three days at room temperature. The supernatant was subsequently recovered for pH and activity measurements at equilibrium. To test the reversibility of ^{210}Pb adsorption and then perform its desorption, between 9 and 10 mL of the two $[Cl]_{tot.}$ solutions (0.027 M or 0.11 M) were added to the remaining clay slurry in the centrifuge tubes, which were shaken for three days before new collection of the supernatant for pH measurements and aqueous analysis. To assess the potential dissolution of smectite during these experiments, especially under acidic conditions, aluminum

concentrations were measured in the supernatants obtained after filtration at 0.1 µm by inductively coupled plasma-atomic emission spectroscopy (ICP-AES, Thermo Scientific® iCAP™ 6000 Series).

The activity of aqueous ^{210}Pb remaining after both adsorption and desorption steps was obtained by gamma ray spectrometric analysis using a coaxial-type germanium detector and was measured by considering the 46.5 keV peak for direct measurement (see more details in Robin et al. (2017) for the geometry used for these activity measurements).

Experimental $K_{d(ads)}$ (adsorption step) was calculated according to Equation 1:

$$K_{d(ads)} = \frac{A_0 - A_{eq_1}}{A_{eq_1}} \times \frac{V_{tot_1}}{m_d} \quad (1)$$

where $K_{d(ads)}$ is the distribution coefficient (mL/g) from the adsorption step, A_0 (Bq/mL) is the initial activity of ^{210}Pb added to the batch, A_{eq_1} (Bq/mL) is the activity of ^{210}Pb measured in the supernatant at equilibrium (Bq/mL), V_{tot_1} (mL) is the volume of solution used for adsorption experiments, and m_d (g) is the mass of dry solid after dehydration at 105 °C.

For the desorption experiments, distribution coefficients (i.e., $K_{d(des)}$) were calculated according to Equation 2:

$$K_{d(des)} = \frac{A_{rem} - A_{eq_2}}{A_{eq_2}} \times \frac{(V_{tot_2} + V_{rem})}{m_d} \quad (2)$$

where $K_{d(des)}$ is the distribution coefficient (mL/g) from the desorption step, A_{rem} is the activity of ^{210}Pb remaining in the clay slurry (i.e., solid + remaining poral solution) after the adsorption step (Bq/mL), and A_{eq_2} is the activity of ^{210}Pb measured in the supernatant at equilibrium after the desorption step (Bq/mL). V_{rem} is the volume of solution remaining in the clay slurry after the adsorption step (mL), V_{tot_2} is the volume of solution added for the desorption step (mL), and m_d (g) is the mass of dry solid after dehydration at 105 °C.

The error calculation is an important step for the comparison between experimental and model data, and each K_d was associated with a minimum error value (ΔK_d) calculated according to the error propagation law (Barrante, 1974):

$$\Delta K_d = \sqrt{\left(\frac{A_i \cdot V_f}{m_d \cdot {A_{eq}}^2}\right)^2 \times Q_{A_{eq}}^2 + \left(\frac{V_f}{m_d \cdot A_{eq}}\right)^2 \times Q_{A_i}^2} \quad (3)$$

where m_d (g) is the same as that parameter defined in Equations 1 and 2. A_i (Bq/mL) and V_f (mL) are equal to A_0 and V_{tot_1}, respectively, in the case of $K_{d(ads)}$ (see Equation 1; adsorption step) and to A_{rem} and to $V_{tot_2} + V_{rem}$, respectively, in the case of $K_{d(des)}$ (see Equation 2;

desorption step). Q_{Ai} is the error associated with A_i: equal to 7 % when $A_i=A_0$ (same uncertainty for each adsorption point), while error corresponds to uncertainty on A_{eq} when $A_i=A_{rem}$ (leading then to different uncertainty for each desorption point). Note that this error calculation method does not consider possible errors in the solid mass and solution volumes; this choice is supported by the small contributions of these two errors (<1 %) in comparison to the errors of activity.

2.3. Thermodynamic calculations and modeling

The approach adopted in this study to interpret lead sorption at various pH values is based on a previous multisite model developed for the solid used here (<0.3 µm of SBId-1), which accounts for the sorption of major cations of natural waters (Na^+, K^+, Mg^{2+}, Ca^{2+}), Al^{3+}, H^+ and trace elements (Ra^{2+}) in Robin et al. (2017 and 2015b).

Experimental ion-exchange isotherms were interpreted using Phreeqc® software (Parkhurst and Appelo, 1999) associated with the Lawrence Livermore National Laboratory (LLNL) thermodynamic database (Johnson et al., 2000), including aqueous complexation constants for Pb(II). To consider the possible aqueous complexation of Ra^{2+}, the LLNL database was augmented by the formation constants of complexes involving radium with chlorides, carbonates, and hydroxyls, as proposed in the Prodata database 1.4 version, which was recently developed (Reiller and Descostes, 2020) to predict water/rock interactions for mining environments. For all simulated data, aqueous activity coefficients were calculated by using the Debye Huckel law, and modeling was performed assuming an equilibrium of the aqueous phase with atmospheric $CO_{2(g)}$ ($10^{-3.5}$ atm.).

The modeling used a multisite approach to fit the experimental data, in which the total CEC of the material was divided into several types of reactive sites, implying that the heterogeneity of the mineral surface properties could be considered (Ly et al., 1991; Reinoso-Maset and Ly, 2016; Tertre et al., 2009). As discussed in Robin et al. (2015b), the model developed on beidellite was built with 3 types of reactive sites (>Xa, >Xb and >Xc), which can potentially be attributed to interlayer sites (>Xa and >Xb) or external sites (>Xc) of the smectite particle. These reactive sites constitute a set of parameters able to best fit the experimental isotherms obtained for the exchange of major cations, including H^+ and Al^{3+} and Ra^{2+} (ultratrace element) at the surface of the beidellite. In this study, the sorption constant characterizing the exchange reaction of two cations (A and B) at each: (i) site on the solid surface was approximated using a selectivity coefficient ($K^i_{A/B}$) and calculated using the equivalent fraction convention (Gaines-Thomas formalism) (Gaines and Thomas, 1953). More details of this modeling procedure can

be found in Tertre et al. (2011a). Modeling performed in this study for the adsorption/desorption of ^{210}Pb was done by considering the ion-exchange of major cations of natural waters (Na^+, Mg^{2+}, Ca^{2+}, K^+), protons, Al^{3+} and radium (Ra^{2+}) at the surface of SBId-1 beidellite previously proposed by Robin et al. (2017, 2015b) (see selectivity coefficients and site concentrations used in Table 1). Note that during the modeling of experimental data, aqueous phases were always undersaturated with respect to Pb(II)- and Ra(II)-bearing phases (such as hydroxides, sulfates, carbonates, chlorides and Fe-Mn oxyhydroxides) and amorphous silica, confirming that ion-exchange reactions were likely to be the unique processes involved for these two elements.

Table 1. a) Site concentrations and associated logarithms of selectivity coefficients (Gaines-Thomas convention) proposed by (Robin et al., 2015b) for five inorganic cations (Na^+, K^+, Mg^{2+}, Ca^{2+} and Al^{3+}), protons (H^+) and radium (Ra^{2+}) on SBId-1 beidellite. The total site concentration was 100 meq/100 g. b) Logarithm of selectivity coefficients (Gaines-Thomas convention) proposed in this study for $Pb^{2+}/2Na^+$ and $PbCl^+/Na^+$ ion-exchange reactions to interpret the lead-proton experimental isotherms obtained in 0.11 M and 0.027 M NaCl for the SBId-1 beidellite. Selectivity coefficients are proposed for equations written as follows (case Na^+/Pb^{2+} for the Xa site): $Pb^{2+} + 2NaXa = Pb(Xa)_2 + 2Na^+$.

a)	Beidellite (SBId-1) (Robin et al., 2017, 2015b)		
Site types	>Xa	>Xb	>Xc
Site concentration (meq/100 g)	38	30	32
log $K_{(Na^+/H^+)}$	0.1	1.7	5.5
log $K_{(2Na^+/Ca^{2+})}$	0.3	0.3	8
log $K_{(2Na^+/Mg^{2+})}$	0.7	0.7	2
log $K_{(Na^+/K^+)}$	0.2	0.2	2.5
log $K_{(3Na^+/Al^{3+})}$	0.64	0.64	0.64
log $K_{(2Na^+/Ra^{2+})}$	1	1.4	2.2
b)	Beidellite SBId-1 - this study		
log $K_{(2Na^+/Pb^{2+})}$	0.6	1.8	3.7
log $K_{(Na^+/PbCl^+)}$	2	2.4	4.5

3. Results and discussion

3.1. Experimental results

Figures 1A and 1B report the experimental K_d for Ra(II) and Pb(II) versus pH for $[Cl]_{tot.}$ of 0.027 M (Figure 1A) and 0.11 M (Figure 1B). Note that the data for both elements were obtained for the same smectite (SBId-1), allowing us to compare their possible behavior. Desorption data follow the same trend as the data of adsorption, suggesting that the process

investigated is reversible for both elements. Under acidic conditions (i.e., pH<2.2), the K_d of ^{210}Pb is close to the K_d of ^{226}Ra, with values of approximately 10^3 L/kg considering error bars for the two $[Cl]_{tot.}$ investigated. The K_d values of Ra(II) and Pb(II) increase with pH irrespective of $[Cl]_{tot.}$ tested, as expected for adsorption of cations on clay minerals (Beneš et al., 1985; Beneš and Strejc, 1986; Fernandes and Baeyens, 2019; Robin et al., 2017; Orucoglu et al., 2018). However, when pH>2.2, $K_d(^{210}Pb)$ is systematically higher than $K_d(^{226}Ra)$, showing that the selectivity of ^{210}Pb is higher than the selectivity of ^{226}Ra for a given pH and $[Cl]_{tot.}$ values. Moreover, for a given pH, the higher the Na concentration is *(i.e. $[Cl]_{tot.}$=0.11 M)*, the lower the $K_d(^{210}Pb)$ and $K_d(^{226}Ra)$ are. Then, all these data indicate that (i) H^+ and Na^+ are competitors of both Ra(II) and Pb(II) for adsorption on the smectite used, and that (ii) there is an ionic strength effect on the adsorption of Pb(II) on smectites, which can be attributed either to competition with Na^+ or to a lower affinity of lead complexes on smectite.

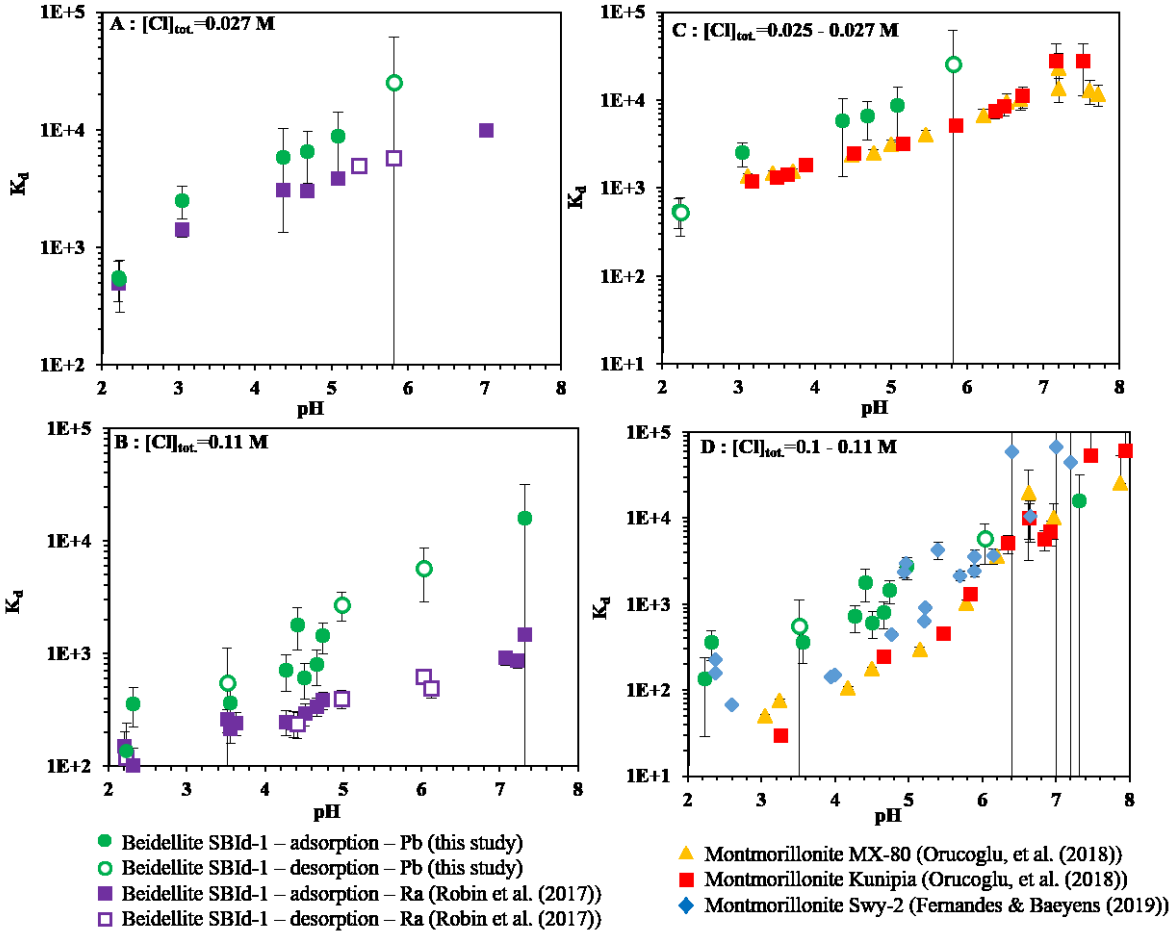

Figure 1: Comparison between K_d measured in this study for Pb(II) adsorption on SBId-1 beidellite with the values reported from the literature for Ra(II) adsorption concomitantly on the same material, for $[Cl]_{tot.}$=0.027 M (A) and 0.11 M (B); and Pb(II) adsorption on montmorillonite for similar total anion concentrations ($[Cl]_{tot.}$=0.025-0.027 M (C); $[Cl]_{tot.}$=0.1-

0.11 M (D)). All K_d values are expressed in L/kg and are reported as a function of pH. Open and filled symbols are obtained from the desorption and adsorption steps, respectively.

Figures 1C and 1D compare $K_d(^{210}Pb)$ measured for Pb(II) in this study for SBId-1, characterized by tetrahedral charge, with the Pb(II) values reported in the literature for montmorillonites characterized by octahedral charges. Figure 1C compares data obtained for similar $[Cl]_{tot.}$ ranging from 0.025 to 0.027 M, while Figure 1D reports data obtained for similar $[Cl]_{tot.}$ ranging from 0.1 to 0.11 M. $K_d(^{210}Pb)$ reported from the literature for montmorillonites increases with increasing pH and decreasing Na^+ concentration. As discussed previously for beidellite, such behavior is due to competition between Pb(II), H^+ and Na^+ on adsorption sites. However, due to experimental errors in K_d, as well as possible variations in CEC, specific surface area (SSA) and mineralogy between SBId-1 and montmorillonites used in the literature, assessment of the possible crystal-chemistry effect (i.e., localization of the charge in the smectite layers) of smectites on $K_d(^{210}Pb)$ values remains to be explored.

3.2. Modeling and associated inputs/outputs

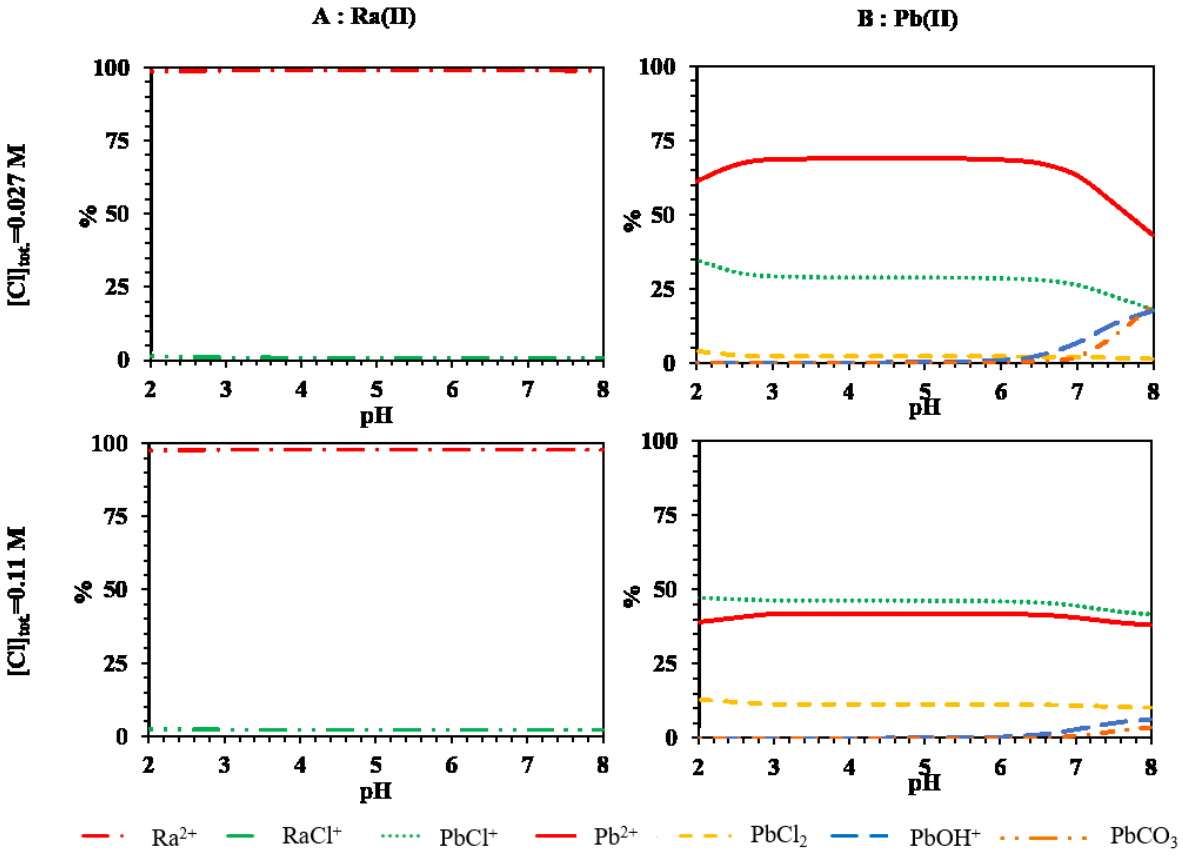

Figure 2: Comparison between aqueous speciation for Ra(II) (A) and Pb(II) (B) calculated as a function of pH and for the two total concentrations of chloride investigated in this study (i.e.,

305 $[Cl]_{tot.}$) and considering an equilibrium with $pCO_{2(g)}=10^{-3.5}$ atm. See material and method for
306 the thermodynamic calculation. Species contributing to less than 1 % of the total concentration
307 are not shown.
308
309 For the two $[Cl]_{tot.}$ investigated, aqueous speciation of Ra(II) and Pb(II) are reported as a
310 function of pH in Figure 2A and 2B, respectively. Ra^{2+} is always the main Ra(II) species
311 irrespective of the pH and $[Cl]_{tot.}$ values, and the contribution of $RaCl^+$ is always negligible
312 (<3 %). The contributions of other aqueous complexes, such as $RaOH^+$, $RaCO_3$, and
313 $Ra(HCO_3)^+$ are also negligible (<0.01 %). In contrast, for pH values ranging from 2.2 to 8, Pb^{2+}
314 is the dominant form for low $[Cl]_{tot.}$ (0.027 M), while a chloride complex ($PbCl^+$) is the main
315 species for high $[Cl]_{tot.}$ (0.11 M). Note, however, that other species contribute significantly to
316 the speciation of Pb(II) at the two $[Cl]_{tot.}$ investigated (e.g., at 0.027 M, $PbCl^+$ can be present at
317 approximately 30 %, while the proportion of Pb^{2+} can reach approximately 45 % at 0.11 M).
318 The contributions of $PbCl_2$, $PbOH^+$ and $PbCO_3$ are always low for pH<7 (<11 %) under our
319 experimental conditions. Other complexes involving Pb(II) ($PbCl_3^-$, $PbCl_4^{2-}$, $Pb(OH)_2$) are
320 always <0.9 % under our experimental conditions. Finally, note that sensitivity tests using
321 aqueous speciation calculations performed with Thermoddem (Blanc et al., 2012) and Prodata
322 (Reiller and Descostes, 2020) thermodynamic databases show Pb(II) speciation (with <6 % of
323 differences; see Figure S.I.1) similar to those obtained with the LLNL (see Figure S.I.1 for the
324 comparison).
325 Pb^{2+} and $PbCl^+$ coexist as the main aqueous Pb(II) species for the two $[Cl]_{tot.}$ investigated.
326 Then, the question arises whether both species, differing by their charge (monovalent for $PbCl^+$
327 and divalent for Pb^{2+}), are involved in Pb(II) sorption. This factor can be assessed by using a
328 method previously proposed by Reinoso-Maset and Ly (2016) to study the sorption of metallic
329 cations, such as Pb(II), that can be present as free divalent cations (Pb^{2+}) and hydroxylated
330 complexes with a lower valence (such as $PbOH^+$). The method considered two parameters, X
331 and Y, specific to each experimental point. X is relative to aqueous measured concentrations
332 (pH and Na^+; see Equation 5) of main competitors of lead for adsorption onto the solid surface,
333 while Y takes into account experimental K_d, aqueous measured concentration of Pb(II) and pH,
334 and computed Pb(II) aqueous speciation (see Equation 6). In the present study, this formalism
335 was adapted to a chloride system to assess the role of Pb^{2+} and $PbCl^+$ in the Pb(II) sorption
336 process. Then, for an aqueous system including H^+, electrolyte cations (e.g., Na^+) and Pb(II)
337 present as different species (Pb^{2+}, $PbCl^+$), two parameters (i.e., X and Y) can be defined:

$$X = log\left(\frac{\gamma_{Na^+}}{\gamma_{H^+}}\frac{[Na^+]}{[H^+]}\right) \quad (5)$$

$$Y = log\ K_{d_M} + log\frac{[^{210}Pb]_T}{[^{210}Pb^{2+}]} - log\left(\frac{\gamma_{Pb^{2+}}}{\gamma_{H^+}^2} \times \frac{1}{[H^+]^2}\right) \quad (6)$$

in which γ_{Na^+} and γ_{H^+} are the molar activity coefficients of the ionic species and K_{d_M} is the measured experimental K_d (in L/kg) as defined in Equations 1 and 2 for the adsorption and desorption steps, respectively, in this study. [ ] is the concentration of the aqueous species (in M): $[^{210}Pb]_T$ was calculated by considering aqueous measured Pb activities; $[H^+]$ is related to the measured pH; $[Na^+]$ is related to Na^+ concentration; each $[^{210}Pb^{2+}]$ used was calculated by using aqueous speciation simulated by PhreeqC® specific to all experimental data obtained.

From the analysis of the slope of Y = f(X), Reinoso-Maset and Ly (2016) succeeded in assessing the valence of the aqueous species that are adsorbed by considering that a slope equal to -1 corresponds to the adsorption of a monovalent cation (as $PbCl^+$ in our case), and a slope equal to -2 corresponds to adsorption of a divalent cation (Pb^{2+} here), as presented in Figure 3 for the two $[Cl]_{tot.}$ investigated. The slopes obtained are -1.56 and -1.48 for $[Cl]_{tot.}$ equal to 0.027 M and 0.11 M, respectively. This behavior suggests that adsorption of both divalent and monovalent Pb(II) species (Pb^{2+} and $PbCl^+$) probably occurs for both $[Cl]_{tot.}$ conditions. These results are in agreement with previous results showing the significant adsorption of chloride complexes (such as $PbCl^+$) on clay minerals for similar $[Cl]_{tot.}$ (Charlet and Tournassat, 2005; Tertre et al., 2011a, 2011b; Tournassat et al., 2004 ; Wang et al., 2015). Then, the adsorption of both Pb^{2+} and $PbCl^+$ will be considered in the modeling procedure of experimental K_d.

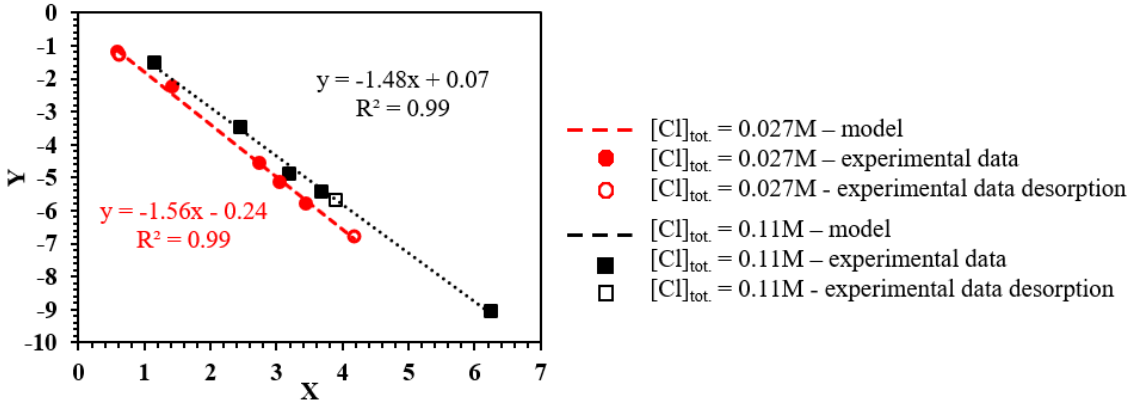

Figure 3: Input and output of the sorption model. Experimental data (symbols) reported by using the (X, Y) representation (see text for details) for $[Cl]_{tot.}$ equal to 0.027 M and 0.11 M, allowing linear regression (dashed lines) of each of the two datasets to assess the valence of the adsorbed species. Because the regression slopes are not integral numbers (such as 1 or 2), the assumption that a minimum of two adsorbed species differing by their valence (e.g., one monovalent and

363 one divalent) can be reasonably proposed as input parameters in the model (see text for more
364 explanations).
365
366 The maximum measured concentration for aqueous aluminum was obtained for pH ~2.2 and
367 was equal to approximately $5 \cdot 10^{-5}$ M; note in addition that measurements were higher than the
368 quantification limits only for samples having pH <4. The value obtained for pH ~2.2
369 corresponded to a maximum percentage of dissolution of approximately 0.3 wt %, suggesting
370 that we can reasonably assume that the site concentrations are constant irrespective of the pH
371 range investigated here. Furthermore, note that interpretation of the Pb(II), H^+ and Na^+
372 exchange was made by considering the aqueous aluminum concentration measured for each
373 specific pH and the $3Na^+/Al^{3+}$ selectivity coefficients (see Table 1 for values from the literature
374 data).

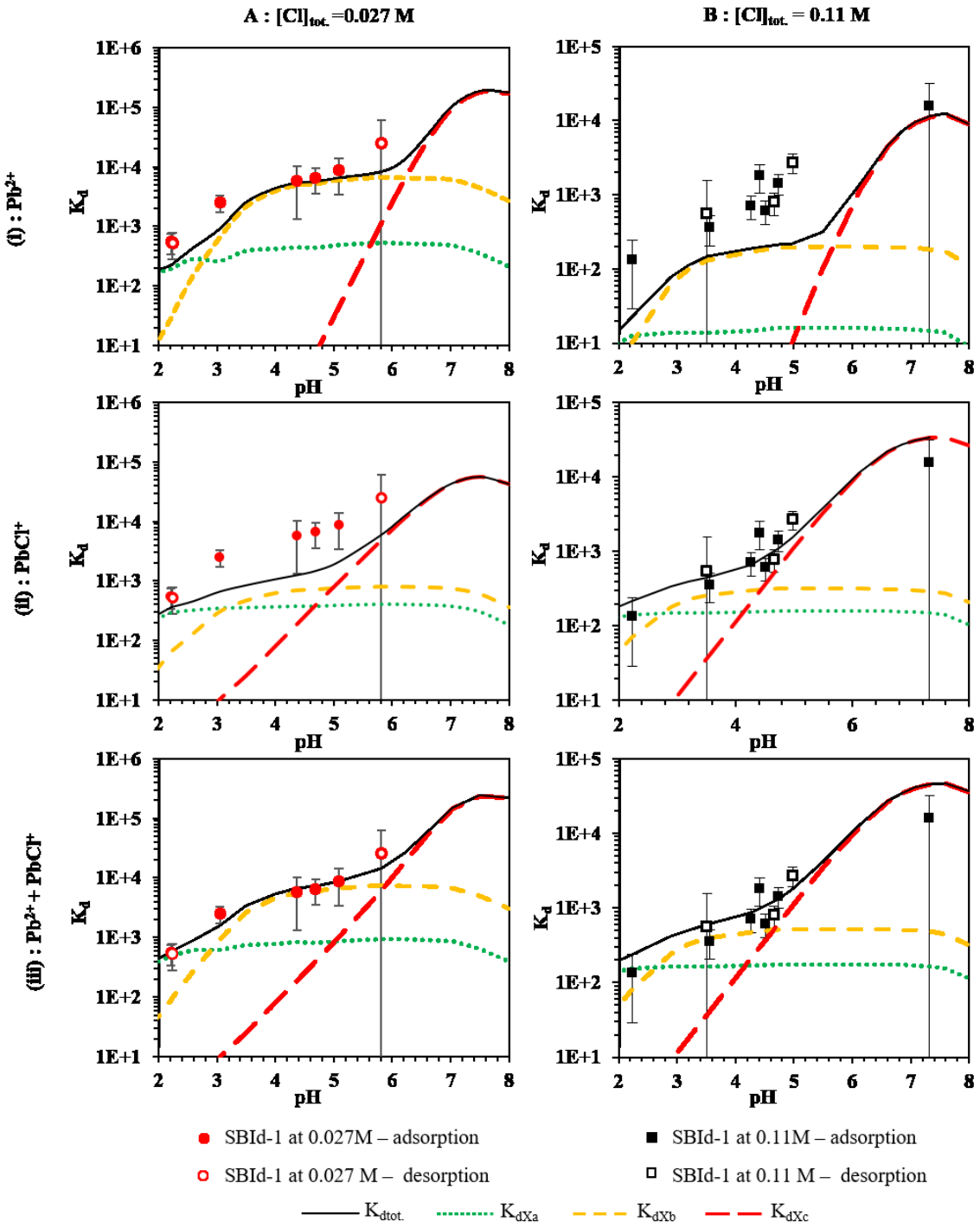

Figure 4: Comparison between experimental K_d (in L/kg) as a function of pH obtained in this study with the values calculated by considering the ion-exchange model proposed. Data are reported for $[Cl]_{tot.}$ 0.027 M (A) and 0.11 M (B). Modeled adsorbed Pb^{2+} and $PbCl^{+}$ contributions and total adsorbed Pb(II) are reported in (i), (ii) and (iii), respectively (full lines). The contributions of the three sites to the total concentrations of adsorbed Pb(II), calculated by the model, are reported in the figures as dashed lines. For experimental data, open and filled symbols are obtained from the desorption and adsorption steps, respectively.

By considering only the adsorption of Pb^{2+}, the general shape of the experimental isotherms was not correctly reproduced, while experimental data were better modeled by introducing exchange of $PbCl^{+}$ (see comparison between experimental data and modeled data in Figure 4). Thus, selectivity coefficient values involving Na^{+}, Pb^{2+} and $PbCl^{+}$ on each adsorption site (>Xa, >Xb and >Xc) allow us to interpret the whole dataset (i.e., at the two $[Cl]_{tot.}$ investigated) and are reported in Table 1. Note that site concentrations are constant, with a distribution identical to previous studies on major and trace elements (Robin et al., 2017, 2015b), and that only the selectivity coefficient values were adjusted.

Table 2: Experimental conditions used in this study and in the literature to study the sorption of Pb(II) on smectites.

Smectite	**CEC (meq/100 g)**	**$[Cl]_{tot.}$ (M)**	**Solid/liquid ratio (g/L)**	**Pb(II) (M)**	**References**
Beidellite SBId-1 <0.3 µm	100	0.027 0.11	2.78	10^{-11}	This study
Montmorillonite Kunipia	78	0.025 0.1	0.5 1.01	10^{-6}	(Orucoglu et al., 2018)
Montmorillonite MX-80	78	0.025 0.1	0.5 1.01	10^{-6}	(Orucoglu et al., 2018)
Montmorillonite Swy-2	87	0.1	1.1	10^{-10}	(Fernandes and Baeyens, 2019)

Finally, the capability of the model proposed in this study to interpret experimental data reported from the literature (Fernandes and Baeyens, 2019; Orucoglu et al., 2018) for the sorption of Pb(II) on different smectites was tested. For these modeling procedures, the total concentrations of Pb(II) and CEC proposed by the authors were used for the calculations (see Table 2). The same distribution of the three sites include in the model (>Xa, >Xb and >Xc) that those proposed in this study for beidellite were assumed to simulate literature data. First, Figure 5 compares: experimental data reported by (Fernandes and Baeyens, 2019) for sorption of ultratrace Pb(II) (see Table 2) on the Swy-2 montmorillonite obtained as a function of pH for a $[Cl]_{tot.}$=0.1 M, with those predicted here with the model proposed. A good agreement can be observed between the two data sets. This shows the rather good capacity of our model, based on three major sites and considering the competition between Pb(II) (i.e., Pb^{2+} and $PbCl^{+}$), Al^{3+}, H^{+} and Na^{+} species, to reproduce experimental data from the literature obtained with other smectites (montmorillonite). Figure 5B and 5C compare prediction with experimental data

reported by Orucoglu et al. (2018) for sorption of trace Pb(II) (see Table 2) on Kunipia and MX-80 (materials rich in montmorillonite) for different $[Cl]_{tot.}$ In these cases, shapes of the experimental dataset are rather well reproduced as a function of pH for the different conditions investigated. However, the predicted data systematically overestimate the experimental data even though the CEC proposed by the authors was used as input for the calculations, suggesting that parameters other than CEC can be at the origin of these discrepancies, such as: (i) differences in the total Pb(II) aqueous initial concentration (10^{-11}/10^{-10} M vs 10^{-6} M) inducing potential site saturation and/or precipitation, and (ii) the presence or absence of other major (from mineral dissolution at lower pH) or trace competitors inherent to work with natural clays (as divalent metals) for sorption sites.

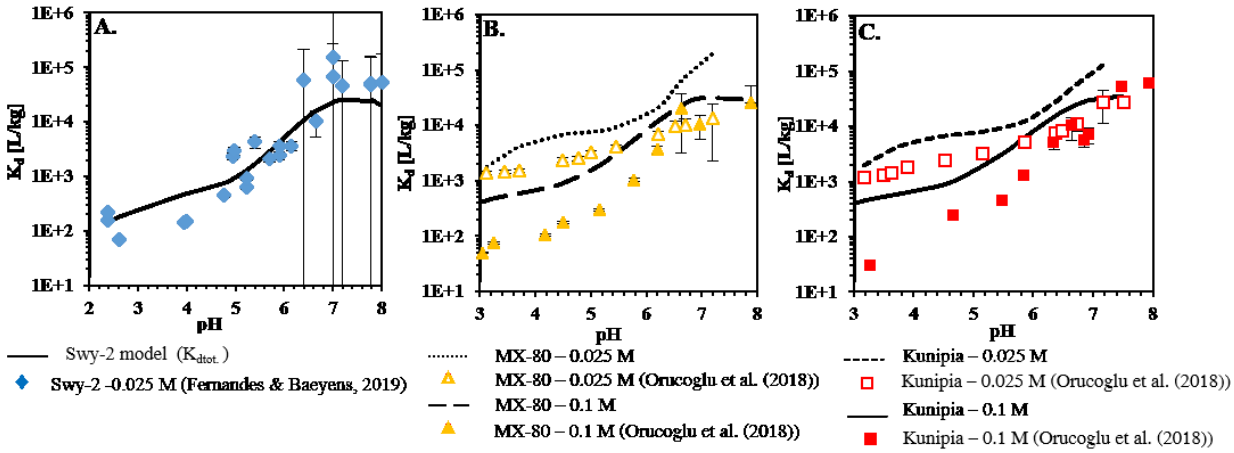

Figure 5 : Comparison between experimental K_d reported from literature (A. Fernandes and Baeyens (2019) and B. and C. Orucoglu et al., 2018; symbols) for adsorption of Pb(II) on swelling clay rich materials with those predicted by the ion-exchange model proposed in this study (see Table 1; line). Open symbols correspond to $[Cl]_{tot.}$=0.025 M and filled correspond to $[Cl]_{tot.}$=0.1 M.

For the predictions, the total concentrations of sites proposed by the authors equal to 87 meq/100 g for Swy-2 (Fernandes and Baeyens (2019)) and 78 meq/100 g for MX-80 and Kunipia (Fernandes and Baeyens, 2019) (Table 2) have been taken into account, and were distributed between the three sites proposed in the model. The same selectivity coefficients between montmorillonite and beidellite were considered to assess the validity of the proposed model to other swelling clay than beidellite.

3.3. Implication for ^{226}Ra(II)/^{210}Pb(II) disequilibrium in natural environments

Since the ^{226}Ra and ^{210}Pb adsorption experiments on the swelling clay were performed at the same time in a single set of batch experiments, performing a direct comparison of the behavior of Ra(II) and Pb(II) is relevant. As the ^{226}Ra/^{210}Pb ratio is used in many environmental and dating applications, knowing if ion exchange reactions in a wide range of waters physico-chemical conditions (pH from 2.2 to 7.3 and ionic strengths of 0.027 M and 0.11 M) may have an effect on the two isotopes distribution between solid and solution is of prime interest. Thus, the aqueous ratios of activities of ^{226}Ra and ^{210}Pb measured at thermodynamic equilibrium of the exchange reaction, normalized to the ratio of initial activities of both elements, allowing to discuss their relative behavior with respect to adsorption at the smectite surface, are reported as a function of pH for two ionic in Figure 6.

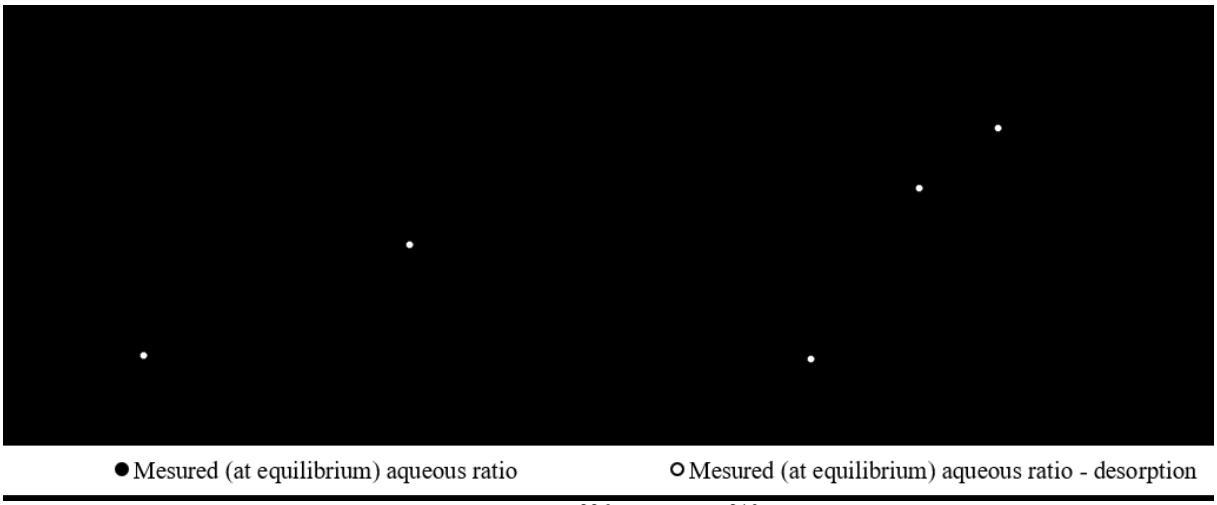

Figure 6: Aqueous ratio of activities of ^{226}Ra and ^{210}Pb measured at equilibrium (A_{eq} corresponding to A_{eq1} and A_{eq2} for the adsorption step (Equation 1) and the desorption step (Equation 2), respectively), normalized by the initial activity of both elements (A_i corresponding to A_0 and A_{rem} for the adsorption step (Equation 1) and the desorption step (Equation 2), respectively). The data are plotted as a function of pH and for the two $[Cl]_{tot.}$ investigated (A: 0.027 M; B: 0.11 M). Open and filled symbols are obtained from the desorption and adsorption steps, respectively.

Data show that the aqueous phase at equilibrium is systematically enriched in ^{226}Ra compared to ^{210}Pb by comparison to the initial steps, suggesting a drastically different reactivity between the 2 isotopes**.** Measurements of the concentrations or activity of ^{210}Pb(II) and ^{226}Ra(II) are commonly performed in the literature to obtain natural radioactive disequilibrium values and then to date geological mechanisms as hydrothermal deposits (Pickler et al., 2012) and to age or determine the growth rate of marine organisms (Andrews et al., 2005; Sabatier et al.,

2012). In a wider use, the "excess" of ^{210}Pb with regard to ^{226}Ra in soils and surface sediments is used for tracing and dating purposes (Mabit et al., 2014). Indeed, these two isotopes are often in disequilibrium with an excess of ^{210}Pb due to aerial deposition of lead-bearing particles, the lead originating from decay of ^{222}Rn released in the atmosphere. In such contexts, systems are often considered to be closed (or with constant flux regarding excess ^{210}Pb), and the possible difference of sorption behaviour of both radionuclides are rarely quantified (especially for the same material) (Appleby and Oldfield, 1992; He and Walling, 1996; Porcelli and Swarzenski, 2003). Thus, in all these applications, the "differential" exchange between solid and solution of radium and lead may interfere with the recorded signal from the U and Th decay series. For instance, the quantity of ^{210}Pb in excess with regard to ^{226}Ra for dating recent sedimentary deposits or tracing soil erosion processes can be miscalculated, as if, as in the experiments presented here, the radium is preferentially released in solution compared to lead during solid-solution interactions, leading to overestimation of lead-excess from aerial deposition. Indeed, the data reported in this study are obtained on the same smectite for these two radionuclides, which allows a direct comparison to discuss the possible difference in behavior between these two isotopes. The data (Figure 1A and B) showed that the K_d of ^{210}Pb measured on the smectite used was higher than the K_d of ^{226}Ra for a given physicochemical condition (pH, $[Cl]_{tot.}$, solid/solution ratio). The same data using the ratio between aqueous ^{226}Ra and ^{210}Pb activity measured at equilibrium are plotted in Figure 6 as a function of pH for the two $[Cl]_{tot.}$. ^{226}Ra aqueous activity is systematically higher than that of ^{210}Pb, in relation to the lower selectivity of Ra(II) over that of Pb(II). These natural radioactive disequilibria increase drastically with pH, up to a factor of 9, over the pH range of 2.2 to 7.3 and for two ionic strengths ($[Cl]_{tot.}$ 0.027 M and 0.11 M). These results could be considered in the future to date geological processes, such as those that may occur in slightly acidic and low carbonate surface or subsurface environments (e.g., acidic soils representing more than 50 % of European soils or surface sediments of catchments with crystalline bedrock) an also in slightly basic pH or high salinity condition as in sea water (i.e., pH=8.2 at 0.5 M for $[Cl]_{tot.}$).

Concluding remarks and perspectives

Experimental data relative to Pb(II) ion-exchange at the ultratrace scale ($<10^{-10}$ mol/L) were obtained on a swelling clay characterized by a tetrahedral charge (beidellite) as a function of pH and for two ionic strengths fixed by NaCl solutions (0.027 and 0.11 M). These data were interpreted by considering aqueous speciation involving Pb^{2+} and ion pairs (as $PbCl^+$ in our case) and a previous ion-exchange model based on three adsorption sites without specific site

for traces elements, including competition with Na^+, H^+ and Al^{3+} cations. The proposed model, based only on three major sites, is able to correctly reproduce the whole dataset for which Pb(II) is adsorbed at the ultratrace scale, as well as previously published data obtained with another swelling clay (i.e., montmorillonite characterized by an octahedral charge). From these results, considering the approach used, no evidence of the localization of the structural charge (tetrahedral vs octahedral) on the adsorption of Pb(II) on low charged swelling clay was established.

Data acquired with ^{210}Pb in this study were obtained on the same swelling clay and during the same experiments as those used for a previous study devoted to ^{226}Ra, allowing discussion without ambiguity of the possible contrast of reactivity between both elements. The results showed that Pb(II) adsorption is preferentially adsorbed over Ra(II) in the physicochemical conditions tested; such contrasting behavior should be considered in the future for geological dating by radioactive disequilibrium ($^{226}Ra(II)/^{210}Pb(II)$).

Acknowledgments

This work was realized with financial support from Orano Mining, and the authors would like to thank the CEA L3MR laboratory for assistance during experiments and measurements.

Supplementary Information

Figure S.I.1 reports a comparison of aqueous speciation calculations performed for Pb(II) with three different thermodynamic databases (i.e., LLNL (Johnson et al., 2000), Thermoddem (Blanc et al., 2012) and Prodata (Reiller and Descostes, 2020)), and the data are plotted as a function of pH for the two $[Cl]_{tot.}$ tested. Species contributing less than 1 % of the total concentration are not shown.

Figure captions

Figure 1: Comparison between K_d measured in this study for Pb(II) adsorption on SBId-1 beidellite with the values reported from the literature for Ra(II) adsorption concomitantly on the same material, for $[Cl]_{tot.}$=0.027 M (A) and 0.11 M (B); and Pb(II) adsorption on montmorillonite for similar total anion concentrations ($[Cl]_{tot.}$=0.025-0.027 M (C); $[Cl]_{tot.}$=0.1-0.11 M (D)). All K_d values are expressed in L/kg and are reported as a function of pH. Open and filled symbols are obtained from the desorption and adsorption steps, respectively.

Figure 2: Comparison between aqueous speciation for Ra(II) (A) and Pb(II) (B) calculated as a function of pH and for the two total concentrations of chloride investigated in this study (i.e., $[Cl]_{tot.}$) and considering an equilibrium with $pCO_{2(g)}=10^{-3.5}$ atm. See material and method for the thermodynamic calculation. Species contributing to less than 1 % of the total concentration are not shown.

Figure 3: Input and output of the sorption model. Experimental data (symbols) reported by using the (X, Y) representation (see text for details) for $[Cl]_{tot.}$ equal to 0.027 M and 0.11 M, allowing linear regression (dashed lines) of each of the two datasets to assess the valence of the adsorbed species. Because the regression slopes are not integral numbers (such as 1 or 2), the assumption that a minimum of two adsorbed species differing by their valence (e.g., one monovalent and one divalent) can be reasonably proposed as input parameters in the model (see text for more explanations).

Figure 4: Comparison between experimental K_d (in L/kg) as a function of pH obtained in this study with the values calculated by considering the ion-exchange model proposed. Data are reported for $[Cl]_{tot.}$ 0.027 M (A) and 0.11 M (B). Modeled adsorbed Pb^{2+} and $PbCl^{+}$ contributions and total adsorbed Pb(II) are reported in (i), (ii) and (iii), respectively (full lines).

Figure 5: Comparison between experimental K_d reported from literature (A. Fernandes and Baeyens (2019) and B. and C. Orucoglu et al., 2018; symbols) for adsorption of Pb(II) on swelling clay rich materials with those predicted by the ion-exchange model proposed in this study (see Table 1; line). Open symbols correspond to $[Cl]_{tot.}$=0.025 M and filled correspond to $[Cl]_{tot.}$=0.1 M.
For the predictions, the total concentrations of sites proposed by the authors equal to 87 meq/100 g for Swy-2 (Fernandes and Baeyens (2019)) and 78 meq/100 g for MX-80 and Kunipia (Fernandes and Baeyens, 2019) (Table 2) have been taken into account, and were distributed between the three sites proposed in the model. The same selectivity coefficients between montmorillonite and beidellite were considered to assess the validity of the proposed model to other swelling clay than beidellite.

Figure 6: Aqueous ratio of activities of ^{226}Ra and ^{210}Pb measured at equilibrium (A_{eq} corresponding to A_{eq1} and A_{eq2} for the adsorption step (Equation 1) and the desorption step

(Equation 2), respectively), normalized by the initial activity of both elements (A_i corresponding to A_0 and A_{rem} for the adsorption step (Equation 1) and the desorption step (Equation 2), respectively). The data are plotted as a function of pH and for the two $[Cl]_{tot.}$ investigated (A: 0.027 M; B: 0.11 M). Open and filled symbols are obtained from the desorption and adsorption steps, respectively.

Table captions

Table 1. a) Site concentrations and associated logarithms of selectivity coefficients (Gaines-Thomas convention) proposed by (Robin et al., 2015b) for five inorganic cations (Na^+, K^+, Mg^{2+}, Ca^{2+} and Al^{3+}), protons (H^+) and radium (Ra^{2+}) on SBId-1 beidellite. The total site concentration was 100 meq/100 g. b) Logarithm of selectivity coefficients (Gaines-Thomas convention) proposed in this study for $Pb^{2+}/2Na^+$ and $PbCl^+/Na^+$ ion-exchange reactions to interpret the lead-proton experimental isotherms obtained in 0.11 M and 0.027 M NaCl for the SBId-1 beidellite.

Table 2: Experimental conditions used in this study and in the literature to study the sorption of Pb(II) on smectites.

References

Appleby, P., and Oldfield, F. (1992). Applications of lead-210 to sedimentation studies. In Uranium-series disequilibrium : Applications to earth, marine, and environmental sciences. 2. Ed.

Andrews, A. H., Cailliet, G. M., Kerr, L. A., Coale, K. H., Lundstrom, C., and DeVogelaere, A. P. (2005). Investigations of age and growth for three deep-sea corals from the Davidson Seamount off central California. In Cold-water corals and ecosystems (p. 1021-1038). Springer. https://link.springer.com/chapter/10.1007/3-540-27673-4_51

Ballini, M., Chautard, C., Nos, J., Phrommavanh, V., Beaucaire, C., Besancon, C., Boizard, A., Cathelineau, M., Peiffert, C., and Vercouter, T. (2020). A multi-scalar study of the long-term reactivity of uranium mill tailings from Bellezane site (France). Journal of environmental radioactivity, 218, 106223. https://doi.org/10.1016/j.jenvrad.2020.106223

Barbier, F., Duc, G., and Petit-Ramel, M. (2000). Adsorption of lead and cadmium ions from aqueous solution to the montmorillonite/water interface. Colloids and Surfaces A: physicochemical and engineering aspects, 166(1-3), 153-159. https://doi.org/10.1016/S0927-7757(99)00501-4

Barrante, J. R. (1974). Applied Mathematics for Physical Chemistry.

Beneš, P., Borovec, Z., and Strejc, P. (1985). Interaction of radium with freshwater sediments and their mineral components: II. Kaolinite and montmorillonite. Journal of radioanalytical and nuclear chemistry, 89(2), 339-351. https://doi.org/10.1007/bf02040598

Beneš, P., and Strejc, P. (1986). Interaction of radium with freshwater sediments and their mineral components: IV. Waste water and riverbed sediments. Journal of radioanalytical and nuclear chemistry, 99(2), 407-422. https://doi.org/10.1007/bf02037602

Berlo, K., and Turner, S. (2010). ^{210}Pb–^{226}Ra disequilibria in volcanic rocks. Earth and Planetary Science Letters, 296(3-4), 155-164 https://doi.org/10.1016/j.epsl.2010.05.023

Besançon, C., Chautard, C., Beaucaire, C., Savoye, S., Sardini, P., Gérard, M., and Descostes, M. (2020). The role of barite in the post-mining stabilization of radium-226: A modeling contribution for sequential extractions. Minerals, 10(6), 497. https://doi.org/10.3390/min10060497

Billon, S., Sardini, P., Angileri, A., Beaucaire, C., Parneix, J. C., Siitari-Kauppi, M., and Descostes, M. (2020). Quantitative imaging of ^{226}Ra ultratrace distribution using digital autoradiography: Case of doped celestines. Journal of environmental radioactivity, 217, 106211. https://doi.org/10.1016/j.jenvrad.2020.106211

Blanc, P., Lassin, A., Piantone, P., Azaroual, M., Jacquemet, N., Fabbri, A., and Gaucher, E. C. (2012). Thermoddem: A geochemical database focused on low temperature water/rock interactions and waste materials. Applied geochemistry, 27(10), 2107-2116. https://doi.org/10.1016/j.apgeochem.2012.06.002

Bordelet, G., Beaucaire, C., Phrommavanh, V., and Descostes, M. (2018). Chemical reactivity of natural peat towards U and Ra. Chemosphere, 202, 651-660. https://doi.org/10.1016/j.chemosphere.2018.03.140

Broecker, W. S., and Peng, T.-H. (1982). Tracers in the Sea (Vol. 690). Lamont-Doherty Geological Observatory, Columbia University Palisades, New York. https://doi.org/10.1016/j.chemosphere.2018.03.140

Charlet, L., and Tournassat, C. (2005). Fe(II)-Na(I)-Ca(II) cation exchange on montmorillonite in chloride medium: Evidence for preferential clay adsorption of chloride–metal ion pairs in seawater. Aquatic Geochemistry, 11(2), 115-137. https://link.springer.com/article/10.1007/s10498-004-1166-5

Curti, E., Fujiwara, K., Iijima, K., Tits, J., Cuesta, C., Kitamura, A., Glaus, M., and Müller, W. (2010). Radium uptake during barite recrystallization at 23±2 C as a function of solution composition: An experimental 133Ba and 226Ra tracer study. Geochimica et Cosmochimica Acta, 74(12), 3553-3570. https://doi.org/10.1016/j.gca.2010.03.018

de Boissezon, H., Levy, L., Jakymiw, C., Distinguin, M., Guerin, F., and Descostes, M. (2020). Modeling uranium and ^{226}Ra mobility during and after an acidic in situ recovery test (Dulaan Uul, Mongolia). Journal of Contaminant Hydrology, 235, 103711. https://doi.org/10.1016/j.jconhyd.2020.103711

Fagbohungbe, M. O., Herbert, B. M., Hurst, L., Ibeto, C. N., Li, H., Usmani, S. Q., and Semple, K. T. (2017). The challenges of anaerobic digestion and the role of biochar in optimizing anaerobic digestion. Waste management, 61, 236-249. https://doi.org/10.1016/j.wasman.2016.11.028

Fernandes, M. M., and Baeyens, B. (2019). Cation exchange and surface complexation of lead on montmorillonite and illite including competitive adsorption effects. Applied Geochemistry, 100, 190-202. https://doi.org/10.1016/j.apgeochem.2018.11.005

Fesenko, S., Carvalo, F., Martin, P., Moore, W. S., and Yankovich, T. (2014). Radium in the environment. The Environmental Behaviour of Radium. International Atomic Energy Agency, Vienna, 33e105. https://www-pub.iaea.org/MTCD/Publications/PDF/trs476_web.pdf

Fu, W., Ram, R., Etschmann, B., Brugger, J., and Vaughan, J. (2020). Selective impurity removal and Cu upgrading of copper flotation concentrate by a spontaneously oxidative H_2SO_4 leaching process. Hydrometallurgy, 195, 105411. https://doi.org/10.1016/j.hydromet.2020.105411

Gailhanou, H., Blanc, P., Rogez, J., Mikaelian, G., Kawaji, H., Olives, J., Amouric, M., Denoyel, R., Bourrelly, S., and Montouillout, V. (2012). Thermodynamic properties of illite, smectite and beidellite by calorimetric methods: Enthalpies of formation, heat capacities, entropies and Gibbs free energies of formation. Geochimica et Cosmochimica Acta, 89, 279-301. https://doi.org/10.1016/j.gca.2012.04.048

Gaines Jr, G. L., and Thomas, H. C. (1953). Adsorption studies on clay minerals. II. A formulation of the thermodynamics of exchange adsorption. The Journal of Chemical Physics, 21(4), 714-718. https://doi.org/10.1063/1.1698996

Ghaleb, B. (2009). Overview of the methods for the measurement and interpretation of short-lived radioisotopes and their limits. 5(1), 012007. https://iopscience.iop.org/article/10.1088/1755-1307/5/1/012007/pdf

Grozeva, N. G., Radwan, J., Beaucaire, C., and Descostes, M. (2022). Reactive transport modeling of U and Ra mobility in roll-front uranium deposits-: Parameters influencing ^{226}Ra/^{238}U disequilibria. Journal of Geochemical Exploration, 236, 106961. https://doi.org/10.1016/j.gexplo.2022.106961

Hanor, J. S. (2000). Barite–celestine geochemistry and environments of formation. Reviews in Mineralogy and Geochemistry, 40(1), 193-275. https://doi.org/10.2138/rmg.2000.40.4

He, Q., and Walling, D. (1996). Interpreting particle size effects in the adsorption of ^{137}Cs and unsupported ^{210}Pb by mineral soils and sediments. Journal of Environmental Radioactivity, 30(2), 117-137. https://doi.org/10.1016/0265-931X(96)89275-7

Hem, J. D. (1976). Geochemical controls on lead concentrations in stream water and sediments. Geochimica et Cosmochimica Acta, 40(6), 599-609. https://doi.org/10.1016/0016-7037(76)90106-X

Ivanovich, M., and Harmon, R. S. (1992). Uranium-series disequilibrium: Applications to earth, marine, and environmental sciences. 2.

Johnson, J., Anderson, G., and Parkhurst, D. (2000). Database from 'thermo. Com. V8. R6. 230'prepared at Lawrence Livermore National Laboratory, (Revision: 1.11).

Kelebemang, R., Dinake, P., Sehube, N., Daniel, B., Totolo, O., and Laetsang, M. (2017). Speciation and mobility of lead in shooting range soils. Chemical Speciation and Bioavailability, 29(1), 143-152. https://doi.org/10.1080/09542299.2017.1349552

Lacal, J., da Silva, M. P., García, R., Sevilla, M. T., Procopio, J. R., and Hernandez, L. (2003). Study of fractionation and potential mobility of metal in sludge from pyrite mining and affected river sediments: Changes in mobility over time and use of artificial ageing as a tool in environmental impact assessment. Environmental Pollution, 124(2), 291-305. https://doi.org/10.1016/S0269-7491(02)00461-X

Langmuir, D., and Riese, A. C. (1985). The thermodynamic properties of radium. Geochimica et cosmochimica acta, 49(7), 1593-1601. https://doi.org/10.1016/0016-7037(85)90264-9

Lestini, L., Beaucaire, C., Vercouter, T., Ballini, M., and Descostes, M. (2019). Role of trace elements in the 226-Radium incorporation in sulfate minerals (gypsum and celestite). ACS Earth and Space Chemistry, 3(2), 295-304. https://doi.org/10.1021/acsearthspacechem.8b00150

Love, M. S., Yoklavich, M. M., Black, B. A., and Andrews, A. H. (2007). Age of black coral (Antipathes dendrochristos) colonies, with notes on associated invertebrate species. Bulletin of Marine Science, 80(2), 391-399.

Ly, J., Stammose, D., and Pitsch, H. (1991). Description of actinides sorption onto clays by ion exchange mechanisms. Migration, 91.

Mabit, L., Benmansour, M., Abril, J., Walling, D., Meusburger, K., Iurian, A., Bernard, C., Tarján, S., Owens, P., and Blake, W. (2014). Fallout ^{210}Pb as a soil and sediment tracer in catchment sediment budget investigations: A review. Earth-Science Reviews, 138, 335-351. https://doi.org/10.1016/j.earscirev.2014.06.007

MacKenzie, A., Logan, E., Cook, G., and Pulford, I. (1998). Distributions, inventories and isotopic composition of lead in 210Pb-dated peat cores from contrasting biogeochemical environments: Implications for lead mobility. Science of the Total Environment, 223(1), 25-35. https://doi.org/10.1016/S0048-9697(98)00302-7

Marani, D., Macchi, G., and Pagano, M. (1995). Lead precipitation in the presence of sulphate and carbonate: Testing of thermodynamic predictions. Water Research, 29(4), 1085-1092. https://doi.org/10.1016/0043-1354(94)00232-V

Mbadcam, J. K., Anagho, S. G., and Nsami, J. N. (2011). Kinetic and equilibrium studies of the adsorption of lead (II) ions from aqueous solution onto two Cameroon clays: Kaolinite and smectite. Journal of Environmental Chemistry and Ecotoxicology, 3(11), 290-297. https://academicjournals.org/journal/JECE/article-full-text-pdf/67417D42045

McBride, M. B. (1994). Environmental Chemistry Of Soil LS. Environmental Chemistry Of Soil LS.

Meunier, A. (2005). Clays. Springer Science and Business Media.

Mhamdi, M., Galai, H., Mnasri, N., Elaloui, E., and Trabelsi-Ayadi, M. (2013). Adsorption of lead onto smectite from aqueous solution. Environmental Science and Pollution Research, 20(3), 1686-1697. https://link.springer.com/article/10.1007/s11356-012-1015-9

Milena-Pérez, A., Piñero-García, F., Benavente, J., Expósito-Suárez, V., Vacas-Arquero, P., and Ferro-García, M. (2021). Uranium content and uranium isotopic disequilibria as a tool to identify hydrogeochemical processes. Journal of Environmental Radioactivity, 227, 106503. https://doi.org/10.1016/j.jenvrad.2020.106503

Moore, W. S., and Krishnaswami, S. (1972). Coral growth rates using ^{228}Ra and ^{210}Pb. Earth and Planetary Science Letters, 15(2), 187-190. https://doi.org/10.1016/0012-821X(72)90059-3

Orucoglu, E., Tournassat, C., Robinet, J.-C., Made, B., and Lundy, M. (2018). From experimental variability to the sorption related retention parameters necessary for performance assessment models for nuclear waste disposal systems: The example of Pb adsorption on clay minerals. Applied Clay Science, 163, 20-32. https://doi.org/10.1016/j.clay.2018.07.003

Pabalan, R. T., and Turner, D. R. (1996). Uranium (6+) sorption on montmorillonite: Experimental and surface complexation modeling study. Aquatic Geochemistry, 2(3), 203-226. https://link.springer.com/article/10.1007/BF01160043

Parkhurst, D. L., and Appelo, C. A. J. (1999). User's guide to PHREEQC version 2: A computer program for speciation, batch-reaction, one dimensional transport and inverse geochemical calculations. USGS, Water-resources investigations report 99-4259. http://acamedia.info/sciences/J_G/references/PHREEQC_Manual.pdf

Persson, B. R. R., and Holm, E. (2011). Polonium-210 and lead-210 in the terrestrial environment: A historical review. International Topical Meeting on Polonium and Radioactive Lead Isotopes, 102(5), 420-429. https://doi.org/10.1016/j.jenvrad.2011.01.005

Pickler, C., Pinti, D. L., Ghaleb, B., Garduno, V.-H., and Tremblay, A. (2012). Radium depletion and 210Pb/226Ra disequilibrium of Marítaro hydrothermal deposits, Los Azufres geothermal field, Mexico. Geochemical Journal, 46(6), 493-504. https://doi.org/10.2343/geochemj.2.0228

Porcelli, D., and Swarzenski, P. W. (2003). The behavior of U-and Th-series nuclides in groundwater. Reviews in Mineralogy and Geochemistry, 52(1), 317-361.

Powell, K. J., Brown, P. L., Byrne, R. H., Gajda, T., Hefter, G., Leuz, A.-K., Sjöberg, S., and Wanner, H. (2009). Chemical speciation of environmentally significant metals with inorganic ligands. Part 3: The Pb^{2+} OH^-, Cl^-, CO_3^{2-}, SO_4^{2-}, and PO_4^{3-}systems (IUPAC Technical Report). Pure and Applied Chemistry, 81(12), 2425-2476. https://doi.org/10.1351/PAC-REP-09-03-05

Ram, R., Morrisroe, L., Etschmann, B., Vaughan, J., and Brugger, J. (2021). Lead (Pb) sorption and co-precipitation on natural sulfide, sulfate and oxide minerals under environmental conditions. Minerals Engineering, 163, 106801. https://doi.org/10.1016/j.mineng.2021.106801

Reiller, P. E., and Descostes, M. (2020). Development and application of the thermodynamic database PRODATA dedicated to the monitoring of mining activities from exploration to remediation. Chemosphere, 251, 126301. https://doi.org/10.1016/j.chemosphere.2020.126301

Reinoso-Maset, E., and Ly, J. (2016). Study of uranium (VI) and radium (II) sorption at trace level on kaolinite using a multisite ion exchange model. Journal of environmental radioactivity, 157, 136-148. https://doi.org/10.1016/j.jenvrad.2016.03.014

Rihs, S., Lascar, E., Pourcelot, L., Calmon, P., Redon, P., Galy, C., Turpault, M., Pelt, E., and Chabaux, F. (2021). U-and Th-series disequilibria in separated soil mineral fractions: Insight into the mechanism and timescale of U, Th and Ra redistribution. Chemical Geology, 583, 120455. https://doi.org/10.1016/j.chemgeo.2021.120455

Robin, V., Beaufort, D., Tertre, E., Reinholdt, M., Fromaget, M., Forestier, S., de Boissezon, H., and Descostes, M. (2020). Fate of dioctahedral smectites in uranium roll front deposits exploited by acidic In Situ Recovery (ISR) solutions. Applied Clay Science, 187, 105484. https://doi.org/10.1016/j.clay.2020.105484

Robin, V., Tertre, E., Beaucaire, C., Regnault, O., and Descostes, M. (2017). Experimental data and assessment of predictive modeling for radium ion-exchange on beidellite, a swelling clay mineral with a tetrahedral charge. Applied Geochemistry, 85, 1-9. https://doi.org/10.1016/j.apgeochem.2017.07.009

Robin, V., Hebert, B., Beaufort, D., Sardini, P., Tertre, E., Regnault, O., and Descostes, M. (2015a). Occurrence of authigenic beidellite in the Eocene transitional sandy sediments of the Chu-Saryssu basin (South-Central Kazakhstan). Sedimentary geology, 321, 39-48. https://doi.org/10.1016/j.sedgeo.2015.03.004

Robin, V., Tertre, E., Beaufort, D., Regnault, O., Sardini, P., and Descostes, M. (2015b). Ion exchange reactions of major inorganic cations (H^+, Na^+, Ca^{2+}, Mg^{2+} and K^+) on beidellite: Experimental results and new thermodynamic database. Towards a better prediction of contaminant mobility in natural environments. Applied Geochemistry, 59, 74-84. https://doi.org/10.1016/j.apgeochem.2015.03.016

Sabatier, P., Reyss, J.-L., Hall-Spencer, J. M., Colin, C., Frank, N., Tisnerat-Laborde, N., Bordier, L., and Douville, E. (2012). ^{210}Pb-^{226}Ra chronology reveals rapid growth rate of Madrepora oculata and Lophelia pertusa on world's largest cold-water coral reef. Biogeosciences, 9(3), 1253-1265. https://doi.org/10.5194/bg-9-1253-2012

Sajih, M., Bryan, N., Livens, F., Vaughan, D., Descostes, M., Phrommavanh, V., Nos, J., and Morris, K. (2014). Adsorption of radium and barium on goethite and ferrihydrite: A kinetic and surface complexation modelling study. Geochimica et Cosmochimica Acta, 146, 150-163. https://doi.org/10.1016/j.gca.2014.10.008

Serpaud, B., Al-Shukry, R., Casteignau, M., and Matejka, G. (1994). Adsorption des métaux lourds (Cu, Zn, Cd et Pb) par les sédiments superficiels d'un cours d'eau : Rôle du pH, de la température et de la composition du sédiment. Revue des sciences de l'eau/Journal of Water Science, 7(4), 343-365. https://doi.org/10.7202/705205ar

Tabelin, C. B., Silwamba, M., Paglinawan, F. C., Mondejar, A. J. S., Duc, H. G., Resabal, V. J., Opiso, E. M., Igarashi, T., Tomiyama, S., and Ito, M. (2020). Solid-phase partitioning and release-retention mechanisms of copper, lead, zinc and arsenic in soils impacted by artisanal and small-scale gold mining (ASGM) activities. Chemosphere, 260, 127574. https://doi.org/10.1016/j.chemosphere.2020.127574

Tertre, E., Beaucaire, C., Coreau, N., and Juery, A. (2009). Modelling Zn (II) sorption onto clayey sediments using a multi-site ion-exchange model. Applied Geochemistry, 24(10), 1852-1861. https://doi.org/10.1016/j.apgeochem.2009.06.006

Tertre, E., Prêt, D., and Ferrage, E. (2011a). Influence of the ionic strength and solid/solution ratio on Ca(II)-for-Na^+ exchange on montmorillonite. Part 1: Chemical measurements, thermodynamic modeling and potential implications for trace elements geochemistry. Journal of Colloid and Interface Science, 353(1), 248-256. https://doi.org/10.1016/j.jcis.2010.09.039

Tertre, E., Ferrage, E., Bihannic, I., Michot, L., and Prêt, D. (2011b). Influence of the ionic strength and solid/solution ratio on Ca(II)-for-Na^+ exchange on montmorillonite. Part 2: Understanding the effect of the m/V ratio. Implications for pore water composition and element transport in natural media. Journal of Colloid and Interface Science, 363(1), 334-347. https://doi.org/10.1016/j.jcis.2011.07.003

Tournassat, C., Greneche, J.-M., Tisserand, D., and Charlet, L. (2004). The titration of clay minerals: I. Discontinuous backtitration technique combined with CEC measurements. Journal of colloid and interface science, 273(1), 224-233. https://doi.org/10.1016/j.jcis.2003.11.021

Uddin, M. K. (2017). A review on the adsorption of heavy metals by clay minerals, with special focus on the past decade. Chemical Engineering Journal, 308, 438-462. https://doi.org/10.1016/j.cej.2016.09.029

Vigier, N., Bourdon, B., Turner, S., and Allègre, C. J. (2001). Erosion timescales derived from U-decay series measurements in rivers. Earth and Planetary Science Letters, 193(3-4), 549-563. https://doi.org/10.1016/S0012-821X(01)00510-6

Wang, J., Xia, S., and Yu, L. (2015). Structure and bonding nature of [$PbCl^+$] adsorption on the kaolinite (0 0 1) surface in aqueous system. Applied Surface Science, 330, 411-417. https://doi.org/10.1016/j.apsusc.2015.01.003

Wang, J., Zhong, Q., Baskaran, M., and Du, J. (2019). Investigations on the time-series partitioning of ^{210}Pb, ^{207}Bi and ^{210}Po between marine particles and solution under different salinity and pH conditions. Chemical Geology, 528, 119275. https://doi.org/10.1016/j.chemgeo.2019.119275

Yin, J., Deng, C., Yu, Z., Wang, X., and Xu, G. (2018). Effective removal of lead ions from aqueous solution using nano illite/smectite clay : Isotherm, kinetic, and thermodynamic modeling of adsorption. Water, 10(2), 210. https://doi.org/10.3390/w10020210

Zhao, C., Wang, C., Hong, H., Algeo, T. J., Yin, K., Ji, K., Song, B., Abels, H. A., and Christidis, G. E. (2021). Origin of dioctahedral smectites in Lower Eocene Lulehe Formation paleosols (Qaidam Basin, China). Applied Clay Science, 203, 106026. https://doi.org/10.1016/j.clay.2021.106026

Zhu, C. (2004). Coprecipitation in the barite isostructural family: 1. Binary mixing properties. Geochimica et Cosmochimica Acta, 68(16), 3327-3337. https://doi.org/10.1016/j.gca.2003.10.014